Steric influences on the photophysical properties of pyrene-based derivatives; mechanochromism and their pH-responsive ability

Jin Zeng[1], Xiaohui Wang[1], Xinyi Song[1], Yiwei Liu[1], Baiyi Liao[1], Jie Bai[1*], Carl Redshaw[2], Qing Chen[3*], Xing Feng[1,4*]

[1]Guangdong Provincial Key Laboratory of Information Photonics Technology. School of Material and Energy, Guangdong University of Technology, Guangzhou 510006, P. R. China.

[2]Department of Chemistry, University of Hull, Cottingham Road, Hull, Yorkshire HU6 7RX, U.K.

E-mail: hyxhn@sina.com (X. Feng), baijie6@gdut.edu.cn (J. Bai)

[3]Chinese Research Academy of Environmental Sciences, No.8, Dayangfang, Beiyuan, Beijing, P. R. China. E-mail: chen.qing@craes.org.cn (Q. Chen)

[4]Guangdong Provincial Key Laboratory of Luminescence from Molecular Aggregates (South China University of Technology) Guangzhou 510640, China.

Keywords: Pyrene, steric effect, structure-property relationship, aggregation-induced emission, pH-responsive

Abstract: Steric effects have attracted great attention in the fields of synthetic chemistry, spectroscopy, crystallography, as well as surface chemistry. Herein, two pyrene-based compounds with different cyclic ketones acting as a bridge are presented and the influence of the steric effects on the luminescent and molecular packing is investigated. Both luminogens display different optical properties in dilute and aggregate states. Notably, the pyrene-based cyclopentanone (**2**) possesses non-aggregation-induced emission (AIE)-active, whilst pyrene-based cyclohexanone (**3**) is AIE-active due to steric effects. Furthermore, the mechanochromism properties and pH-responsive ability of both pyrenes were investigated by use of fluorescence spectra.

The present work provides insight into how steric effects impact on the molecular conformations and optical properties in these new pyrene-based AIE luminogen systems.

Introduction

The concept of "aggregation-induced emission (AIE)", coined by Tang and coworkers in 2001 [1], is considered one of the top 10 emerging technologies in chemistry according to International Union of Pure and Applied Chemistry (IUPAC) reports [2]. Organic luminescent materials with AIE characteristics have attracted increased interest both in the academic community and industry, and this has led to advances in flexible organic electronic devices [3-6], fluorescent probes [7], chemsensors [8], and clinical medicine [9, 10]. Such work takes advantage of the variety of molecular structures, the tunable-color emission properties, as well as the flexible molecular skeleton [11]. A typical AIE luminogen (AIEgen) exhibits higher fluorescence intensity in the aggregate state compared to in solution state, due to suppression of the non-radiative decay pathways via restricted intramolecular motions (RIM) [5, 12]. In general, the molecules in the aggregate state display a completely different set of chemical/physical properties and performance compared to their behavior in solution, which is due to weak inter-/intramolecular interactions (such as van der Waals' forces, π-π interactions). [13], molecular packing, as well as molecular conformations [14]. For example, hexaphenylbenzene is AIE-active, but pyrene-based asymmetric hexaarylbenzenes display decreased fluorescence intensity, due to the molecular aggregation effect overwhelming the AIE effect [15]. On the other hand, according to the RIM mechanism, a tradition fluorophore is easily transformed into an AIEgens by decorating the twisted bulky units via molecular tailoring strategies [16]. Zhao *et al* have reported a set of pyrene-based AIE blue emitters for potential application in non-doped electroluminescence devices [17-20]. Moreover, Li *et al* have reported six pyrene-based AIEgens by introducing bulky aromatic substituents at the 2,7-positions of the pyrene core, which exhibited high-performance non-doped OLED

properties with high external quantum efficiencies of 3.46% [21]. Our group has reported new pyrene-based cyanostyrene compounds with AIE characteristics and mechanochromism [22, 23].

It has been noted that subtle changes in molecular structures can lead to marked differences in optical/electronical properties [24]. For example, the Schiff-base aggregation-induced emission luminogens (AIEgen) with an -OH group exhibited a red fluorescence color via an excited-state intramolecular proton transfer (ESIPT) process, but in the absence of an -OH group, this did not occur [25]. In the pyrene system, the simple planar molecule 4-bpin-2,7-di-*tert*-butylpyrene displayed dual monomer-excimer-mechanoluminescence and excimer-mechanochromism(MC), whereas 4-bromo-2,7-di-tertbutyl-pyrene is mechanoluminescence-active, which is ascribed to the different molecular packing [26].

In general, the optical properties of organic materials are closely related to their molecular structure [27]. For example, to regulate the emission color of molecules, many feasible strategies have been explored to prepare highly efficient emitters of various colors. For example, strategies include adjusting the length of the π-conjugation in the molecular skeleton, as well as constructing dipolar molecules via requisite selection of donor/acceptor components [28-30]. Moreover, the molecular conformation not only plays a significant role on the optical behavior, but also can affect the biological activity of drug molecules, particularly chiral molecules [31, 32].

We note however that there are few reports that focus on how sterics can influence photophysical properties both in solution and in the aggregate state, and how mechanochromism properties, as well as morphology can influence such properties. With this in mind, this article presents cyclopentanone-/ cyclohexanone-bridged pyrene-based compounds, which display different optical properties both in solution and in the aggregate state. The mechanochromism behavior and pH-responsive ability of the systems are also reported. The influence of the steric effects on the luminescence and molecular packing of this pyrene chemistry is discussed.

Experimental

Materials:

Unless otherwise stated, all reagents used were purchased from commercial sources and were used without further purification. Tetrahydrofuran was distilled prior to use. 7-(*tert*-butyl)pyrene-1-carbaldehyde was synthesized following the previously reports [33, 34].

Characterization

^{1}H and ^{13}C NMR spectra (400 MHz or 600MHz) were recorded on a Bruker AV 400M or AVANCE III 600M spectrometer using chloroform-*d* solvent and tetramethylsilane as internal reference. *J*-values are given in Hz. The ^{1}H NOESY NMR experiments were acquired by the standard three-pulse sequence or by the PFG version. High-resolution mass spectra (HRMS) were taken on a LC/MS/MS, which consisted of a HPLC system (Ultimate 3000 RSLC, Thermo Scientific, USA) and a Q Exactive Orbitrap mass spectrometer. UV-vis absorption spectra and photoluminescence (PL) spectra were recorded on a Shimadzu UV-2600 and the Hitachi F-4700 spectrofluorometer. PL quantum yields were measured using absolute methods using a Hamamatsu C11347-11 Quantaurus-QY Analyzer. The lifetime was recorded on an Edinburgh FLS 980 instrument and measured using a time-correlated single-photon counting method. Thermogravimetric analysis was carried on a Mettler ToledoTGA/DSC3+ under dry nitrogen at a heating rate of 10 ºC/min. The quantum chemistry calculations were performed using the Gaussian 09 (B3LYP/6–311G (d,p) basis set) software package.

Synthesis of (2E,5E)-2,5-bis((7-(*tert*-butyl)pyren-1-yl)methylene)cyclopentanone (2)

A mixture of 7-(*tert*-butyl)pyrene-1-carbaldehyde (160 mg, 0.56 mmol, 2 eq.), cyclopentanone (20.6 mg, 0.24 mmol, 1eq.) and sodium hydride (60 mg, 1.5 mmoL,

1.5 eq) in anhydrous ethanol (5 mL) was stirred and refluxed overnight under nitrogen. After cooling to room temperature, the mixture was filtered and washed twice with ethanol. The residue was further crystallized from THF and hexane to give a yellow powder (73 mg, yield 48 %). Melting point: 279~282 °C, FT-IR (KBr, cm^{-1}): 3442, 3026 (Py ν_{C-H}), 1697 ($\nu_{C=O}$), 1607 (Py $\nu_{C=C}$), 1593 ($\nu_{C=C}$), 1219, 1202, 982, 870, 845, 809, 723, 579 cm^{-1}. ^{1}H NMR (400 MHz, $CDCl_3$) δ 8.78 (s, 2H), 8.58 (d, J = 9.3 Hz, 2H), 8.32 (d, J = 1.7 Hz, 2H), 8.29 (d, J = 1.7 Hz, 2H), 8.24 (d, J = 9.3 Hz, 2H), 8.23 (d, J = 8.1 Hz, 2H), 8.19 (d, J = 8.1 Hz, 2H), 8.14 (d, J = 8.9 Hz, 2H), 8.08 (d, J = 8.9 Hz, 2H), 3.27 (s, 4H), 1.63 (s, 18H) ppm. ^{13}C NMR (101 MHz, $CDCl_3$) δ 195.98, 149.50, 139.60, 131.94, 131.19, 131.07, 130.71, 130.64, 129.55, 128.79, 128.62, 127.21, 126.37, 124.87, 124.37, 123.33, 123.22, 123.16, 122.87, 35.28, 31.92, 27.32 ppm. HRMS (FTMS+p APCI): m/z $+H^+$ calcd for $C_{47}H_{40}O$ 621.3152, found 621.3147 $[M+H]^+$.

Synthesis of (2E,6E)-2,6-bis((7-(*tert*-butyl)pyren-1-yl)methylene)cyclohexanone (3)

A mixture of 7-(*tert*-butyl)pyrene-1-carbaldehyde (160 mg, 0.56 mmol, 2eq.), cyclohexanone (23 mg, 0.23 mmol, 1eq.) and sodium hydride (60 mg, 1.5 mmoL, 1.5 eq) in anhydrous ethanol (5 mL) was stirred and refluxed overnight under nitrogen. After cooling to room temperature, the mixture was filtered and washed twice with ethanol. The residue was further crystallized from THF and hexane to give yellow block crystals (85 mg, yield 60%). Melting point: 315~317 °C, ^{1}H NMR (400 MHz, $CDCl_3$) δ 8.77 (s, 2H), 8.32 (d, J = 9.2 Hz, 2H), 8.28 (d, J = 1.7 Hz, 2H), 8.26 (d, J = 1.7 Hz, 2H), 8.17 (d, J = 9.3 Hz, 2H), 8.16 (d, J = 7.9 Hz, 2H), 8.10 (d, J = 9.0 Hz, 2H), 8.06 (d, J = 8.9 Hz, 2H), 7.99 (d, J = 7.9 Hz, 2H), 3.02 – 2.86 (m, 4H), 1.81 – 1.72 (m, 2H), 1.60 (s, 18H). ppm. FT-IR (KBr, cm^{-1}): 3432, 3051 (Py ν_{C-H}), 1666 ($\nu_{C=O}$), 1617 (Py $\nu_{C=C}$), 1592 ($\nu_{C=C}$), 1360, 1222, 1225, 1172, 1143, 877, 848, 816, 709, 681, 591 cm^{-1}. ^{13}C NMR (101 MHz, $CDCl_3$) δ 190.41, 149.38, 138.28, 135.93, 131.35, 131.16, 130.77, 130.39, 129.79, 128.29, 128.24, 127.21, 126.65, 124.73, 124.15, 124.05, 122.96,

122.90, 35.28, 31.94, 29.00, 23.70 ppm. HRMS (FTMS+p APCI): m/z $+H^+$ calcd for $C_{48}H_{42}O$ 635.3308, found 635.3299 $[M+H]^+$.

Results and Discussion

Synthesis

The detailed synthetic route for the pyrene-based compounds **2**-**3** is outlined in Scheme 1, and shows a classical condensation reaction of 7-(*tert*-butyl)pyrene-1-carbaldehyde (**1**) and the corresponding ketone (cyclopentanone or cyclohexanone) in dry ethanol affording the products in 48 % yield for **2**, and 60 % for **3**, respectively. The chemical structure of the prepared compounds **2** and **3** were fully identified by $^1H/^{13}C$ NMR spectroscopy and high-resolution mass spectrometry. Meanwhile, ^1H-^1H NOESY experiments were further used for confirming the molecular conformation of compounds **2** and **3** as the *E,E*-configuration (Figures S5-S6). The thermogravimetric analysis (TGA) shows that the decomposition temperature (T_d, 5% weight loss) is 361 °C for both compounds **2** and **3**, respectively (Figure S7).

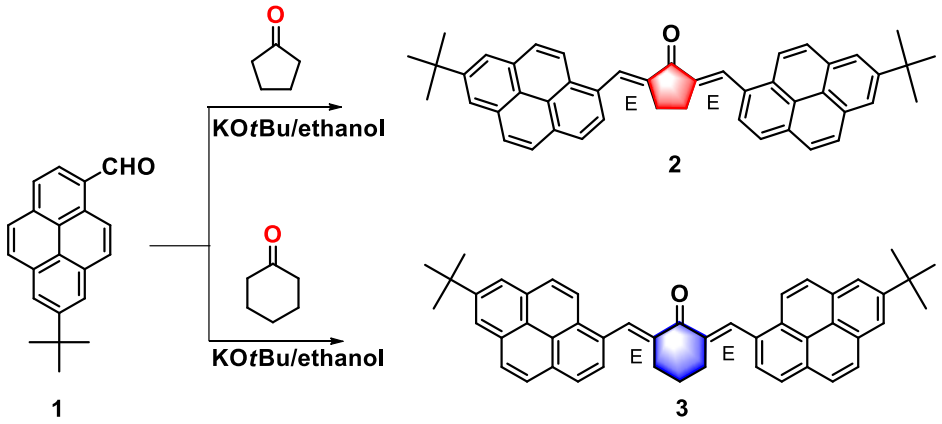

Scheme 1. The synthetic route to the pyrene-based compounds **2** and **3**.

FT-IR spectra

The FT-IR spectra of starting compound **1**, and pyrene-based compounds **2** and **3** were measured and are illustrated in Figure S12. The characteristic vibration peaks of C=O is observed at 1673 cm^{-1}, and a peak at 2723 cm^{-1} is assigned to the stretching vibration of the C−H bonds of the -CHO group of compound **1**. Given the tensile force in

cyclopentanone is larger than in cyclohexanone, the vibration peak of C=O group in compound **2** was shifted to a higher wavenumber. Indeed, the typical vibration peak of the C=O group appeared at 1697 cm^{-1} for **2** and 1666 cm^{-1} for **3**, respectively. Meanwhile, the peak at 2723 cm^{-1} completely disappeared, which indicated that the -CHO group has completely reacted in the condensation reaction. On the other hand, compared to the -CHO group, the typical vibration peak of the C=O group in compound **2** was shifted to higher wavenumber, while that for compound **3** was shifted to lower wavenumber, indicating that compound **2** displayed a higher degree of π-conjugation, which is consistent with our theoretical calculations.

Photophysical properties

The UV-vis spectra of the pyrene-based compounds **2** and **3** were investigated in dilute THF solvent (~10^{-5} M). As shown in Figure 1, both compounds display dominant absorption bands in the ranges 250-300 nm and 350-500 nm, and the short-wavelength absorption peak at 276 nm is assigned to the $S_4 \leftarrow S_0$ transition [35], with similar molar extinction coefficients for compounds **2** and **3**. Meanwhile, the maximum long-wavelength absorption peak of compound **2** is red-shifted to 446 nm with a large molar extinction coefficient, and the long-wavelength absorption peak of compound **3** is at 388 nm, which indicates that compound **2** is more conjugated than compound **3**. This may be due to **2** exhibiting a more coplanar molecular structure, which leads to better electronic communication ability across the bridging cyclopentanone and the pyrene core.

Further, the geometrical parameters of compounds **2** and **3** were optimized by density functional theory (DFT) calculations using the B3LYP function with 6-311G (d,p) basis sets, and were performed to investigate the electronic configuration in the ground state. As shown in Figures S13-S4, the electronic energy of the *E,E*-configuration of compounds **2** and **3** is lower than others, which is consistent with the ^{1}H-^{1}H NOSEY NMR experimental results. Obviously, both molecules adopt a nonplanar structure with a twist angle between the pyrene core with the bridging units

(cyclopentanone or cyclohexanone) in the range 42.06-42.37° for **3**, which is larger than compound **2** (35.82~35.88 °), implying that the bridge unit of cyclohexanone can increase the steric effect. On the other hand, the HOMO levels of compounds **2** and **3** are mainly located at the one of the pyrene units, and the LUMO orbital distribution of electron density is dominant from the bridge unit to a partial pyrene moiety at the other side. The separated HOMO and LUMO distributions of electron density indicated that both compounds are bipolar molecules and that the cyclopentanone or cyclohexanone unit acts as an electron-withdrawing group and the pyrene acts as an electron-donating group [36]. In addition, the energy gap of compounds **2** and **3** are 2.84 eV and 3.11 eV, respectively, indicating that compound **3** exhibits a hypsochromic shifted emission compared to **2**.

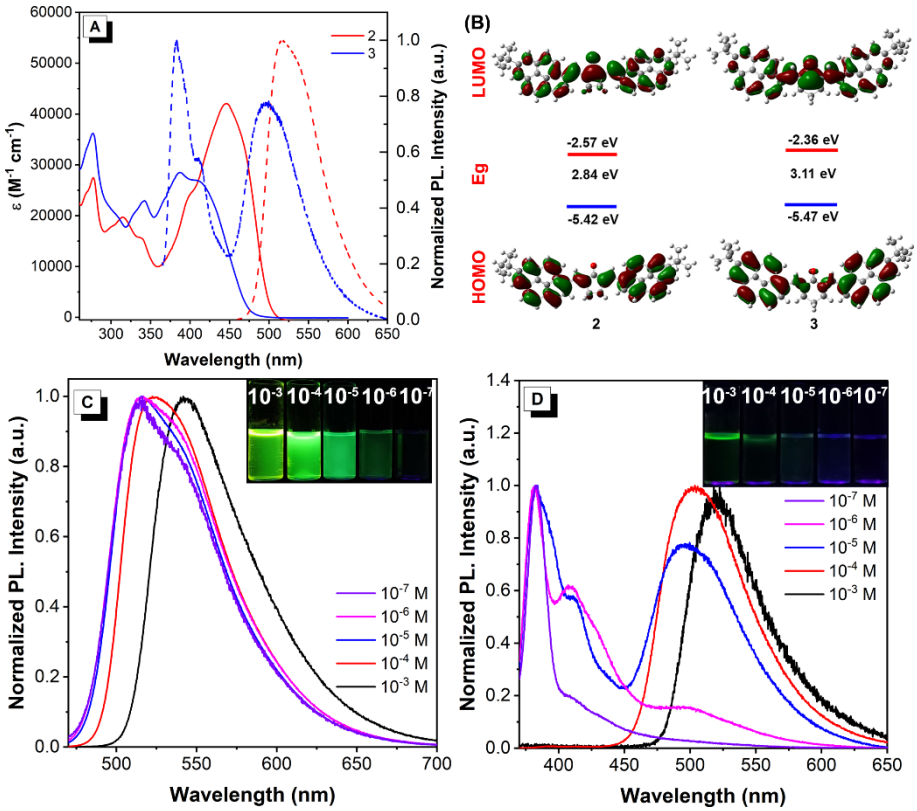

Figure 1. (A) Absorption and emission spectra of **2** and **3** in THF (1.0×10^{-5} M) solution, (B) the HOMOs/LUMOs of **2** and **3** calculated by B3LYP/6-31G*; Concentration-dependent fluorescence spectra of compounds **2** (C) and **3** (D) recorded in THF solvent at 25 °C. Insert: photos of compounds **2** and **3** in THF solution at different concentrations, respectively, taken under 365 nm excitation using a UV lamp.

Upon excitation, compound **2** displays an intense emission with a maximum emission peak at 515 nm, whereas compound **3** displays a dual emission comprising mainly of an emission peak at 383 nm and a shoulder peak at 494 nm in THF solution. The concentration-dependent PL spectra of compounds **2** and **3** in THF solution are presented in Figures 1C and 1D. Compound **2** exhibited a red-shifted emission from 516 nm to 542 nm, as the concentration increased from 10^{-7} to 10^{-3} M, and the fluorescent intensity underwent an enhanced (<10^{-4} M) process, then was quenched in highly concentrated media (10^{-3} M). This may be the result of molecular aggregation at high concentration, leading to a red-shifted emission. On the other hand, the emission wavelength of compound **3** displays a red-shifted emission from 382 nm (in 10^{-7} M) to 518 nm (in 10^{-3} M). The short-wavelength emission peak at 382 nm may originate from the pyrene unit. As the concentration increased, the molecules strengthen their intermolecular interactions resulting in molecular aggregation, leading to excimer emission at 518 nm [37].

Table 1. The photophysical properties of the two pyrene-based cyanostyrene derivatives.

Compd	ε ($\lambda_{max\ abs}$) ($M^{-1}\ cm^{-1}$) [a]	λ_{maxPL} (nm) solns[a]/solid[b]	Φ_f solns[a]/solid[b]	τ (ns) solns[a]/solid[b]	α_{AIE}[c]	K_r ($\times 10^7\ S^{-1}$)[d] solns[a]/solid[b]	K_{nr} ($\times 10^7\ S^{-1}$)[e] solns[a]/solid[b]
2	446/42058	515/561	0.269/0.058	0.9538/1.658	0.216	2.82/0.35	7.66/5.68
3	388/28506	383, 494/517	0.004/0.048	0.31/0.6672	12	0.13/0.72	32.1/14

[a] Maximum absorption wavelength measured in THF solution at room temperature. [b] Measured in solid state, [c] $\alpha = \Phi_{solid}/\Phi_{soln.}$ [d] K_r = radiative decay rate (Φ/τ). [e] K_{nr} = nonradiative decay rate ($1/\tau - k_r$).

Solvatochromic effects

The influence of solvent polarity on the photophysical properties was investigated and results are presented in Figure 2. As the solvent polarity increases from cyclohexane (non-polar solvent) to DMSO (polar solvent), the maximum long-wavelength absorption band was red-shifted from 441 nm (in cyclohexane) to 458 nm (in DMSO) for compound **2**, while compound **3** exhibits a slight red shifted absorption

band from 385 nm to 388 nm. Clearly, the impact of solvatochromism on the absorption spectra of compound **2** is stronger than for compound **3**, indicating that the ground state of the latter is independent of the solvent polarity. On the other hand, with the increase of solvent polarity, compound **2** emits a different emission color from green (511 nm) to orange red (573 nm), and the PL intensity peak was enhanced with a red-shifted emission of 62 nm. This solvent-dependent phenomenon is attributed to the twisted intramolecular charge transfer (TICT) effect. On the other hand, compound **3** displays a weak blue emission with a maximum emission peak of 385 nm in non-polar solvent (in cyclohexane), and as the polarity is increased, the compound exhibits a dual emission. More importantly, the long-wavelength emission was red-shifted from 505 nm to 550 nm with an enhanced emission intensity, which may contribute to the excimer emission [38]. Furthermore, compound **3** dissolved in different solvents, such as cyclohexane, 1,4-dioxane, THF and DMSO at 10^{-3} M, exhibited a maximum emission peak in the range 500 - 554 nm, indicating that compound **3** prefers to form a dimer/trimer at high concentration (Figure S15).

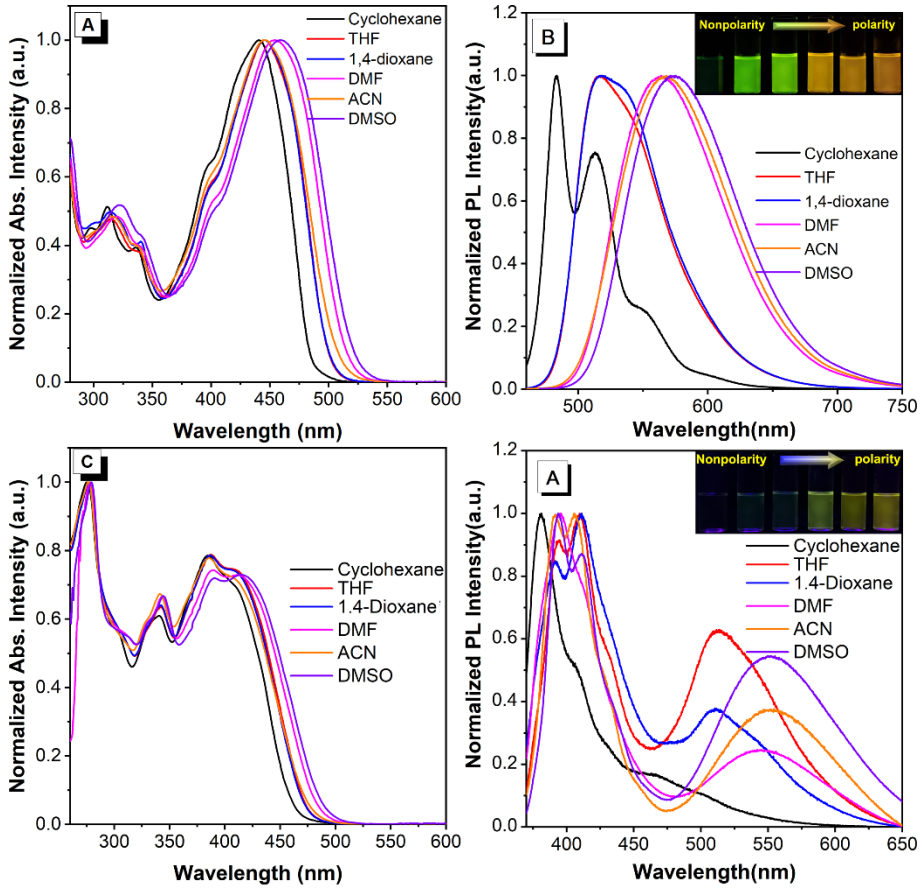

Figure 2. (A) and (C) Normalized Absorption spectra and (B) and (D) Normalized emission spectra of **2** and **3** in different polar solvents (10^{-5} M) solution at 25 °C. Insert: photographs of compounds **2** or **3** in different solvents, respectively, taken under 365 nm excitation of a UV lamp.

AIE characteristic

According to the restricted intramolecular motion (RIM) concept, twisted conformation molecules such as tetraphenylethylene, hexaphenylbenzene and their derivatives such as cyanostyrene derivatives [39] are typical AIEgens or AIEE fluorophores. Some compounds containing a double bond (C=C) also exhibit clear AIE characteristics [40, 41]. Thus, to test the AIE behavior, the PL spectra of the target compounds **2** and **3** were further investigated in mixtures of THF and water with different water fractions (f_w) (Figure 3). As shown in Figure 3C, when the f_w < 60%, compound **3** reveals a weak emission at 392 nm with a shoulder peak at 505 nm, and subsequently, the emission

intensity at λ_{em} =392 nm was enhanced dramatically, and the shoulder emission band was shifted to *ca*. 550 nm when the f_w increased to 60%. After which, the long-wavelength emission was blue-shifted to 460 nm. At the higher water fraction (f_w >80%), the emission intensity has slightly decreased with an enhanced emission peak at 390 nm. The emission peaks of compound **3** at 390 nm, 460 nm and 550 nm correspond to the monomer emission, charge-transfer emission and excimer emission, which undergo a synergetic effect due to the TICT and the molecular aggregation. On the other hand, the quantum yield in THF solution is 0.004 and improved to 0.048 in the solid state. Moreover, the radiative decay rate (K_r) increased from 0.13 $\times 10^7$ S^{-1} in THF to 0.72 $\times 10^7$ S^{-1} in the solid state, while the non-radiative decay rate decreased from 32.1 $\times 10^7$ S^{-1} to 14 $\times 10^7$ S^{-1}, thus, compound **3** is AIE-active. However, the emission peak of compound **2** slowly decreased and was almost quenched as the f_w increased from 0 to 99%, and the fluorescence color was tuned from green (526 nm) to orange (599 nm) ($f_w \leq 50\%$), and then hypsochromically shifted to blue (470 nm). This may be the result of the hydrophobicity of compound **2**, which can exclude the polar water molecules in the aggregate state [42].The quantum yield of compound **2** in solution is higher than in the aggregation state and in the solid state. Thus, compound **2** is a non-AIE molecule.

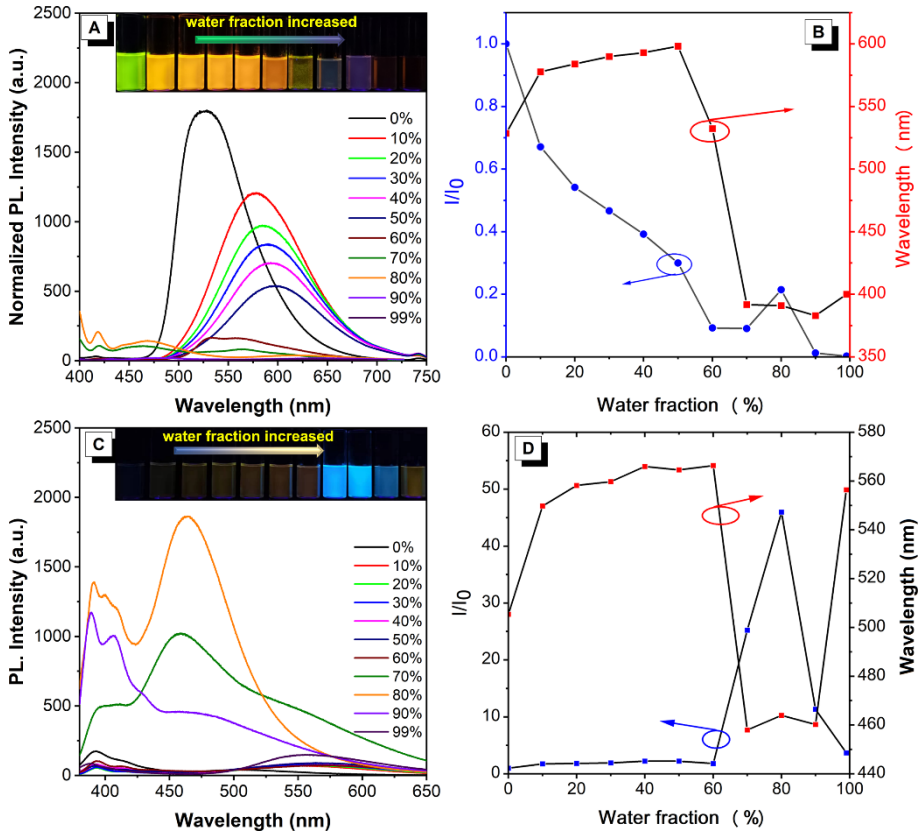

Figure 3. (A) and (C) PL spectra of **2** and **3** in THF/water mixtures with different water fractions (f_w). (B) and (D) The plot of relative PL intensity I/I_0 (blue line) and peak emission wavelength (red line) *versus* f_w. Inset: fluorescent images of **2** and **3** (10^{-5} M) in THF/water mixtures with different f_w taken under 365 nm UV irradiation.

Mechanochromism properties

Both powders of the pyrene-based compounds display yellow emissions with a dual emission band at 535 nm and 560 nm for **2** and the maximum emission peak at 517 nm for **3**. For the pristine powder **2**, upon mechanical grinding, the emission was red-shifted to 607 nm with an emission color change from yellow to orange red. This may be attributed to the excimer emission, and the fluorescence could be recovered to it's original state after treatment with fumes of CH_2Cl_2. Meanwhile, the compound **3** displays a red-shifted emission peak at 542 nm under grinding, and the emission color was changed from green to yellow. The emission can be hypsochromically shifted to 518 nm by CH_2Cl_2 fuming. Although both compounds exhibited an opposite optical phenomenon (one is an ACQ fluorophore, and the other is an AIEgens) in the aggregate

state, they still show reversible mechanical stimuli-response behavior, which may result from the molecular packing in the powdered state.

Powder X-ray diffraction (XRD) was performed to further understand the external stimuli on the emission behavior and the molecular packing. Both compounds **2** and **3** display a sharp and intense diffraction peak, which indicated that both are arranged in a well-ordered crystalline state. The ground samples show weak and broad diffraction signals, implying that the crystalline state was decreased under external stimuli. Moreover, the d-spacing was decreased in the region 2θ = 20-35°, which corresponds to stronger π–π stacking interactions, indicating that the compounds are more planar structure after grinding. While the fumed samples show sharper reflection peaks compared to the grounded samples, suggesting that the molecular structure of the ground and fumed samples are arranged differently, leading to different emission behavior. On the other hand, the PXRD of fumed samples **2** and **3** are same as the their pristine samples.

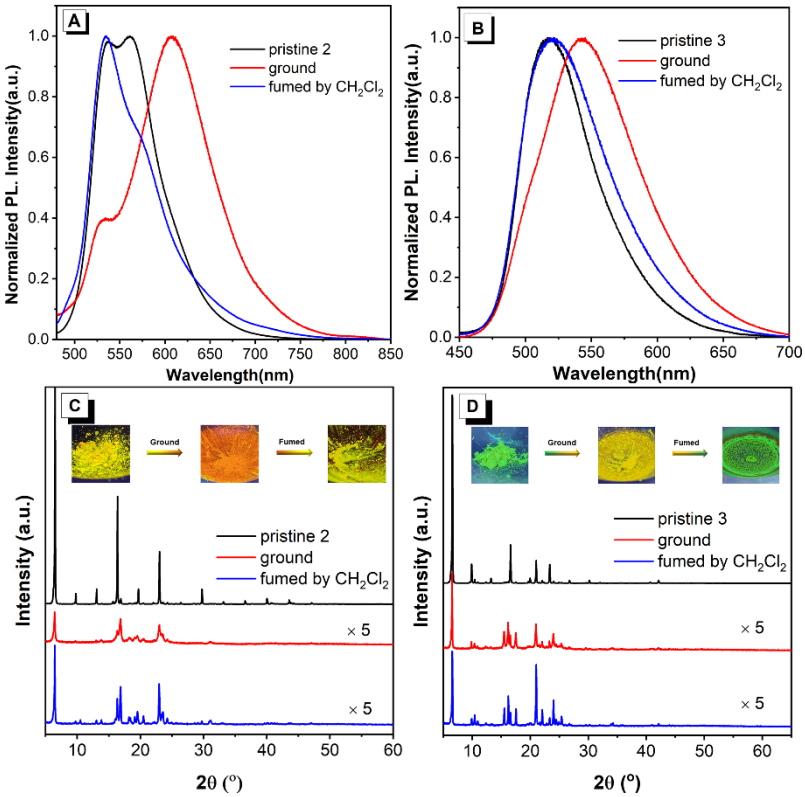

Figure 4. Normalized PL intensity of pyrene-based compound (A) **2** and (B) **3** in three solid states (pristine, ground and fumed by CH_2Cl_2, respectively.) PXRD patterns of three powder states of (C) **2** and (D) **3.** Insert: the fluorescence graphs of **2** and **3** in three powder states under 365 nm UV irradiation.

pH-responsive property

Interestingly, both compounds **2** and **3** also can form a deprotonated state in a strongly acidic atmosphere, leading to a fluorescence quenching process. For example, the pristine powder **3** dissolved in THF (10^{-3} M) and dropped on filter paper, emits intense yellow emission with a maximum emission peak at 560 nm. However, when an amount of hydrochloric acid is dropped onto the filter paper and then air dried at room temperature, the filter paper containing the pristine powder **3** is non-emissive under UV irradiation. When it meets with ammonia solution ($NH_3 \cdot H_2O$), the emission color is changed back to yellow again with an equal emission intensity in a recycling process. Also, compound **2** displayed a similar pH-responsive process, the orange red emission color (600 nm) of the filter paper containing compound **2** was totally quenched once protonated, which could return back again in an ammonia atmosphere with a decreased emission intensity (Figure 5).

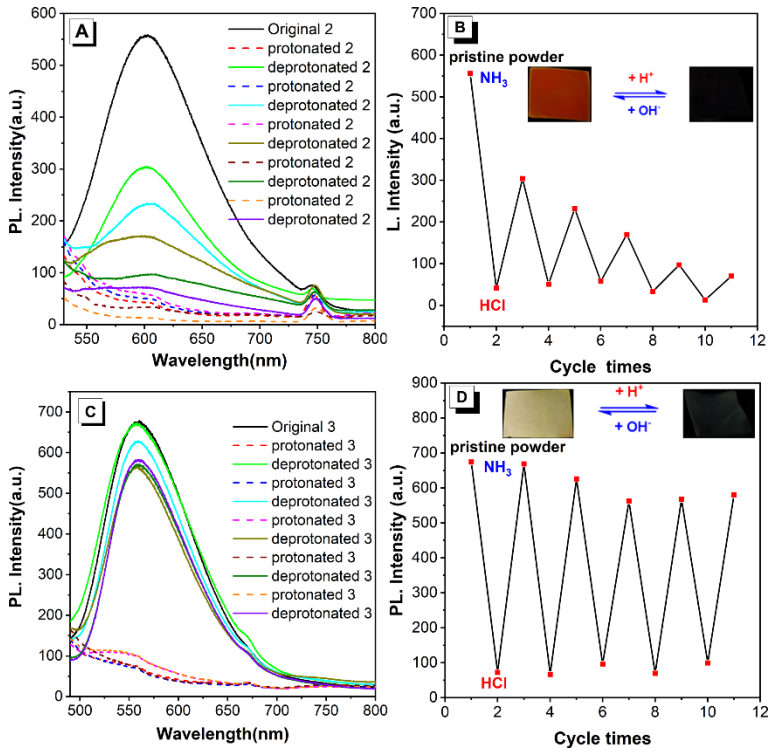

Figure 5. pH-dependent PL spectra of (A) compounds **2** and (C) **3** on filter paper using the protonation-deprotonation process. Switching of the emission wavelength (B) compound **2** and (D) compound **3** by repeated protonation and deprotonation.

Previously, Tang *et al*. reported that 4-(dimethylamino)styryl)quinoxalin-2(1*H*)-one displayed pH-responsive behavior via protonation of the -NMe_2 group, leading to a clear TICT process [43]. Xu *et al*. reported a pH-sensitive single fluorescence compound with AIE and excited state intramolecular proton transfer (ESIPT) features for anti-counterfeiting and food freshness detection [44]. When the tetraphenylethylene scaffold contains a carboxyl group, it can react with amine vapors to realize fluorescence emission changes [45]. To understand the pH-responsive mechanism, the UV-vis and PL spectrum of compounds **2** and **3** at different pH values in solution was investigated. Slightly changed optical behavior over a wide pH range (1 to 13) was observed. However, the fluorescence intensity of both compounds was gradually quenched upon trifluoroacetic acid (TFA) addition from 0 to 1400 μL, which indicated that both compounds can be protonated by TFA, suggesting that the carbonyl unit can be protonated in strongly acidic solvent, but not weakly acidic solvent [Figure S16].

Conclusion

In summary, two pyrene-based compounds with different cyclic ketone bridging groups were designed and synthesized in order to investigate the impact of steric effects on the optical properties, both in solution and in the aggregation state. The slightly different molecular conformations result in opposite optical properties, and compound **2** containing cyclopentanone is non-AIE active, while compound **3** with cyclohexanone is AIE-active. Moreover, compound **2** displays a TICT process, leading to an emission color change from blue to orange red, but compound **3** in highly polar solvent exhibits a charge-transfer emission. In addition, both display multi-stimuli-responsive properties, such as external stimuli and pH-responsive ability, which means such systems could have uses as highly sensitive chemosensors for acidic solvent, and possible optical data storage. Thus, this work presents a notable example of the influence of steric effects on fluorescence behavior and molecular conformations, and also provides a novel molecular design strategy for accessing pyrene-based aggregation-induced emission luminogens.

Acknowledgements

This work was supported by the National Natural Science Foundation of China (Fund NO. 21975054), Natural Science Foundation of Guangdong Province of China (Fund NO. 2019A1515010925), Guangdong Provincial Key Laboratory of Information Photonics Technology (Fund NO. 2020B121201011), the National Key Research and Development Program of China (2021YFC3201501), the Open Fund of Guangdong Provincial Key Laboratory of Luminescence from Molecular Aggregates, Guangzhou 510640, China (South China University of Technology) (Fund NO. 2019B030301003), Science and Technology Planning Project of Hunan Province (Fund NO. 2018TP1017), Budget Surplus of Central Financial Science and Technology Plan (2021-JY-04), CR thanks the EPSRC for an Overseas Travel Grant (EP/R023816/1).

References

[1] Luo J, Xie Z, Lam JW, Cheng L, Chen H, Qiu C, et al. Aggregation-induced emission of 1-methyl-1,2,3,4,5-pentaphenylsilole. Chem Commun (Camb). 2001(18):1740-1. https://doi.org/10.1039/b105159h

[2] Zhao Z, Zhang H, Lam JWY, Tang BZ. Aggregation-Induced Emission: New Vistas at the Aggregate Level. Angew. Chem. Int. Ed. 2020;59(25):9888-907. https://doi.org/10.1002/anie.201916729

[3] Yu Y, Cang M, Cui W, Xu L, Wang R, Sun M, et al. Efficient red fluorescent OLEDs based on aggregation-induced emission combined with hybridized local and charge transfer state. Dyes Pigm. 2021;184:108770. https://doi.org/10.1016/j.dyepig.2020.108770

[4] Tu L, Xie Y, Li Z, Tang B. Aggregation-induced emission: Red and near-infrared organic light-emitting diodes. SmartMat. 2021;2(3):326-46. https://doi.org/10.1002/smm2.1060

[5] Mei J, Leung NL, Kwok RT, Lam JW, Tang BZ. Aggregation-Induced Emission: Together We Shine, United We Soar! Chem Rev. 2015;115(21):11718-940. https://doi.org/10.1021/acs.chemrev.5b00263

[6] Li L, Zhang J, Yang C, Huang L, Zhang J, Bai J, et al. Stimuli-Responsive Materials from Ferrocene-Based Organic Small Molecule for Wearable Sensors. Small. 2021;17:e2103125. https://doi.org/10.1002/smll.202103125

[7] Han X, Ge F, Xu JL, Bu XH. Aggregation-induced emission materials for nonlinear optics. Aggregate. 2021;2:e28. https://doi.org/10.1002/agt2.28

[8] Ma C, Lu W, Yang X, He J, Le X, Wang L, et al. Bioinspired Anisotropic Hydrogel Actuators with On-Off Switchable and Color-Tunable Fluorescence Behaviors. Adv Funct Mater. 2018;28:1704568. https://doi.org/10.1002/adfm.201704568

[9] Zhong D, Chen W, Xia Z, Hu R, Qi Y, Zhou B, et al. Aggregation-induced emission luminogens for image-guided surgery in non-human primates. Nat Commun. 2021;12:6485. https://doi.org/10.1038/s41467-021-26417-2

[10] Wang HP, Chen X, Qi YL, Huang LW, Wang CX, Ding D, et al. Aggregation-induced emission (AIE)-guided dynamic assembly for disease imaging and therapy. Adv Drug Deliv Rev. 2021;179:114028. https://doi.org/10.1016/j.addr.2021.114028

[11] Yang J, Fang M, Li Z. Organic luminescent materials: The concentration on aggregates from aggregation-induced emission. Aggregate. 2020;1(1):6-18. https://doi.org/10.1002/agt2.2

[12] Peng Q, Shuai ZG. Molecular mechanism of aggregation-induced emission. Aggregate. 2021;2:e91. https://doi.org/10.1002/agt2.91

[13] Lou XY, Yang YW. Aggregation-induced emission systems involving supramolecular assembly. Aggregate. 2020;1(1):19-30. https://doi.org/10.1002/agt2.1

[14] Tu Y, Zhao Z, Lam JWY, Tang BZ. Aggregate Science: Much to Explore in the Meso World. Matter. 2021;4(2):338-49. https://doi.org/10.1016/j.matt.2020.12.005

[15] Liu Y, Mao X, Wang X, Bai J, Zhang J, Feng X, et al. Pyrene-based asymmetric hexaarylbenzene derivatives: Synthesis, crystal structures, and photophysical properties. J. Lumin. 2021;12:118653 https://doi.org/10.1016/j.jlumin.2021.118653

[16] Islam MM, Hu Z, Wang Q, Redshaw C, Feng X. Pyrene-based aggregation-induced emission luminogens and their applications. Materials Chemistry Frontiers. 2019;3(5):762-81. https://doi.org/10.1039/c9qm00090a

[17] Zhao Z, Ye S, Guo Y, Chang Z, Lin L, Jiang T, et al. 1,3,6,8-Tetrakis[(triisopropylsilyl)ethynyl]pyrene: A highly efficient solid-state emitter for non-doped yellow electroluminescence devices. Org. Electron. 2011;12(12):2236-42. https://doi.org/10.1016/j.orgel.2011.09.019

[18] Zhao Z, Chen S, Chan CY, Lam JW, Jim CK, Lu P, et al. A facile and versatile approach to efficient luminescent materials for applications in organic light-emitting diodes. Chem Asian J. 2012;7(3):484-8. https://doi.org/10.1002/asia.201100753

[19] Zhao Z, Chen S, Lam JWY, Wang Z, Lu P, Mahtab F, et al. Pyrene-substituted ethenes: aggregation-enhanced excimer emission and highly efficient electroluminescence. J. Mater. Chem. A. 2011;21(20):7210–6. https://doi.org/10.1039/c0jm04449k

[20] Zhao Z, Chen S, Lam JW, Lu P, Zhong Y, Wong KS, et al. Creation of highly efficient solid emitter by decorating pyrene core with AIE-active tetraphenylethene peripheries. Chem Commun 2010;46(13):2221-3. https://doi.org/10.1039/b921451h

[21] Yang J, Li L, Yu Y, Ren Z, Peng Q, Ye S, et al. Blue pyrene-based AIEgens: inhibited intermolecular π–π stacking through the introduction of substituents with controllable intramolecular conjugation, and high external quantum efficiencies up to 3.46% in non-doped OLEDs. Mater. Chem. Front. 2017;1(1):91-9. https://doi.org/10.1039/c6qm00014b

[22] Wang X, Wang L, Mao X, Wang Q, Mu Z, An L, et al. Pyrene-based aggregation-induced emission luminogens (AIEgens) with less colour migration for anti-counterfeiting applications. J. Mater. Chem. C. 2021; 9(37):12828-38. https://doi.org/10.1039/d1tc03022a

[23] Feng X, Zhang J, Hu Z, Wang Q, Islam MM, Ni J-S, et al. Pyrene-based aggregation-induced emission luminogens (AIEgen): structure correlated with particle size distribution and mechanochromism. J. Mater. Chem. C. 2019;7(23):6932-40. https://doi.org/10.1039/c9tc01665a

[24] Yang Z, Xu C, Li W, Mao Z, Ge X, Huang Q, et al. Boosting the Quantum Efficiency of Ultralong Organic Phosphorescence up to 52 % via Intramolecular Halogen Bonding. Angew Chem Int Ed. 2020;59(40):17451-5. https://doi.org/10.1002/anie.202007343

[25] Hu Z, Zhang H, Chen Y, Wang Q, Elsegood MRJ, Teat SJ, et al. Tetraphenylethylene-based color-tunable AIE-ESIPT chromophores. Dyes Pigm. 2020;175:108175. https://doi.org/10.1016/j.dyepig.2019.108175

[26] Gong Y-B, Zhang P, Gu Y-r, Wang J-Q, Han M-M, Chen C, et al. The Influence of Molecular Packing on the Emissive Behavior of Pyrene Derivatives: Mechanoluminescence and Mechanochromism. Adv. Opt. Mater. 2018;6:1800198. https://doi.org/10.1002/adom.201800198

[27] Voskuhl J, Giese M. Mesogens with aggregation-induced emission properties: Materials with a bright future. Aggregate. 2021; e124. https://doi.org/10.1002/agt2.124

[28] Hu R, Zhang G, Qin A, Tang BZ. Aggregation-induced emission (AIE): emerging technology based on aggregate science. Pure Appl. Chem. 2021 ; 000010151520210503. https://doi.org/10.1515/pac-2021-0503

[29] Zhu L, Zhu B, Luo J, Liu B. Design and Property Modulation of Metal–Organic Frameworks with Aggregation-Induced Emission. ACS Mater. Lett. 2020;3(1):77-89. https://doi.org/10.1021/acsmaterialslett.0c00477

[30] Belmonte-Vázquez JL, Amador-Sánchez YA, Rodríguez-Cortés LA, Rodríguez-Molina B. Dual-State Emission (DSE) in Organic Fluorophores: Design and Applications. Chem. Mater. 2021;33(18):7160-84. https://doi.org/10.1021/acs.chemmater.1c02460

[31] Liu B, Bockmann M, Jiang W, Doltsinis NL, Wang Z. Perylene Diimide-Embedded Double [8]Helicenes. J Am Chem Soc. 2020;142(15):7092-9. https://doi.org/10.1021/ja953578v

[32] Endo Y, Ohno M, Hirano M, Itai A, Shudo K. Synthesis, conformation, and biological activity of teleocidin mimics, benzolactams. A clarification of the conformational flexibility problem in structure-activity studies of teleocidins. J. Am. Chem. Soc. 1996;118(8):1841-55. https://doi.org/10.1021/jacs.0c00954

[33] Takano H, Shiozawa N, Imai Y, Kanyiva KS, Shibata T. Catalytic Enantioselective Synthesis of Axially Chiral Polycyclic Aromatic Hydrocarbons (PAHs) via Regioselective C-C Bond Activation of Biphenylenes. J Am Chem Soc. 2020;142(10):4714-22. https://doi.org/10.1021/jacs.9b12205

[34] Feng X, Hu JY, Redshaw C, Yamato T. Functionalization of Pyrene To Prepare Luminescent Materials-Typical Examples of Synthetic Methodology. Chem.Eur.J. 2016;22:11898-916. https://doi.org/10.1002/chem.201600465

[35] Crawford AG, Dwyer AD, Liu Z, Steffen A, Beeby A, Palsson LO, et al. Experimental and theoretical studies of the photophysical properties of 2- and 2,7-functionalized pyrene derivatives. J Am Chem Soc. 2011;133(34):13349-62. https://doi.org/10.1021/ja2006862

[36] Mao X, Xie F, Wang X, Wang Q, Qiu Z, Elsegood MRJ, et al. Ne Quinoxaline-BasedBlue Emitters: Molecular Structures ,Aggregation-InducedEnhanced Emission Characteristics and OLED Application. Chinese J. Chem. 2021;39(8):2154-62. https://doi.org/10.1002/cjoc.202100157

[37] Wang CZ, Noda Y, Wu C, Feng X, Venkatesan P, Cong H, et al. Multiple Photoluminescence from Pyrene-Fused Hexaarylbenzenes with Aggregation-

Enhanced Emission Features. Asian J. Org. Chem. 2018;7(2):444-50. https://doi.org/10.1002/ajoc.201700563

[38] Zhu L, Qin J, Yang C. Synthesis, photophysical properties, and self-assembly behavior of amphiphilic polyfluorene: unique dual fluorescence and its application as a fluorescent probe for the mercury ion. J. Phys. Chem. B. 2010;114(46):14884-9. https://doi.org/10.1021/jp1071567

[39] Gao J, Tian M, He Y, Yi H, Guo J. Multidimensional-Encryption in Emissive Liquid Crystal Elastomers through Synergistic Usage of Photorewritable Fluorescent Patterning and Reconfigurable 3D Shaping. Adv. Funct. Mater. 2021.2107145. https://doi.org/10.1002/adfm.202107145

[40] Gao M, Su H, Li S, Lin Y, Ling X, Qin A, et al. An easily accessible aggregation-induced emission probe for lipid droplet-specific imaging and movement tracking. Chem Commun (Camb). 2017;53(5):921-4. https://doi.org/10.1039/c6cc09471f

[41] Qi Q, Li C, Liu X, Jiang S, Xu Z, Lee R, et al. Solid-State Photoinduced Luminescence Switch for Advanced Anticounterfeiting and Super-Resolution Imaging Applications. J Am Chem Soc. 2017;139(45):16036-9. https://doi.org/10.1021/jacs.7b07738

[42] Liu S, Zhou X, Zhang H, Ou H, Lam JWY, Liu Y, et al. Molecular Motion in Aggregates: Manipulating TICT for Boosting Photothermal Theranostics. J Am Chem Soc. 2019;141(13):5359-68. https://doi.org/10.1021/jacs.8b13889

[43] Alam P, Leung NLC, Su H, Qiu Z, Kwok RTK, Lam JWY, et al. A Highly Sensitive Bimodal Detection of Amine Vapours Based on Aggregation Induced Emission of 1,2-Dihydroquinoxaline Derivatives. Chem. Eur. J. 2017;23(59):14911-7. https://doi.org/10.1002/chem.201703253

[44] Zhang Q, Yang L, Han Y, Wang Z, Li H, Sun S, et al. A pH-sensitive ESIPT molecule with aggregation-induced emission and tunable solid-state fluorescence multicolor for anti-counterfeiting and food freshness detection. Chem. Eng. J. 2022;428:130986. https://doi.org/10.1016/j.cej.2021.130986

[45] Huang G, Jiang Y, Yang S, Li BS, Tang BZ. Multistimuli Response and Polymorphism of a Novel Tetraphenylethylene Derivative. Adv. Funct. 2019;29(16):1900516. https://doi.org/10.1002/adfm.201900516